Author/s:
Kim, C-J;Ercole, F;Ju, Y;Pan, S;Chen, J;Qu, Y;Quinn, JF;Caruso, F

Title:
Synthesis of Customizable Macromolecular Conjugates as Building Blocks for Engineering Metal–Phenolic Network Capsules with Tailorable Properties

Date:
2021

Citation:
Kim, C. -J., Ercole, F., Ju, Y., Pan, S., Chen, J., Qu, Y., Quinn, J. F. & Caruso, F. (2021). Synthesis of Customizable Macromolecular Conjugates as Building Blocks for Engineering Metal–Phenolic Network Capsules with Tailorable Properties. Chemistry of Materials, 33 (21), https://doi.org/10.1021/acs.chemmater.1c02912.

Persistent Link:
https://hdl.handle.net/11343/290663

# Synthesis of Customizable Macromolecular Conjugates as Building Blocks for Engineering Metal–Phenolic Network Capsules with Tailorable Properties

*Chan-Jin Kim,[†,§] Francesca Ercole,[‡,§] Yi Ju,[†] Shuaijun Pan,[†] Jingqu Chen,[†] Yijiao Qu,[†] John F. Quinn,*[,‡,#] and Frank Caruso*[,†]*

[†]ARC Centre of Excellence in Convergent Bio-Nano Science and Technology, and the Department of Chemical Engineering, The University of Melbourne, Parkville, Victoria 3010, Australia

[‡]ARC Centre of Excellence in Convergent Bio-Nano Science and Technology, Drug Delivery, Disposition and Dynamics Theme, Monash Institute of Pharmaceutical Sciences, Monash University, Parkville, Victoria 3052, Australia

[#]Department of Chemical Engineering, Faculty of Engineering, Monash University, Clayton, Victoria 3800, Australia

*Corresponding authors. E-mail: john.f.quinn@monash.edu (J.F.Q.); fcaruso@unimelb.edu.au (F.C.)

## ABSTRACT

Metal–phenolic networks (MPNs), formed through coordination bonding between phenolic molecules and metal ions, are a promising class of materials for engineering particle systems for diverse applications. However, the properties of such MPNs are inherently restricted due to the finite properties of naturally occurring phenolic molecules. Herein, we report a simple and robust approach to incorporate phenolic moieties into polymers, thereby providing customizable phenolic ligand building blocks that can be used to assemble capsules with a range of tailorable properties. The phenolic ligand building blocks were synthesized via carbonic anhydride coupling to terminal amines, a conjugation approach typically used for peptide coupling but applied herein for functionalizing polymers. The chemistry enabled optimized end group purity, thus affording a robust and efficient strategy to generate a library of macromolecular poly(ethylene glycol) (PEG) catechol building blocks with different architectures (i.e., 2-, 4-, and 8-arm) and molecular weights (from 2.5 to 20 kDa). The resulting phenolic building blocks were applied to fabricate capsules with shell thickness, permeability, and cell association properties that were controlled via variation of the macromolecular catechol architecture and molecular weight. Specifically, shell thickness was varied more than 19-fold (i.e., between 8.7 and 169.3 nm) by judicious selection of the polymer molecular weight, arm number, and template. Similarly, permeability of the resulting MPN capsules to 500 kDa dextran was tuned from >90% to <5% by varying the number of arms in the polymer structure while maintaining a constant PEG $M_n$-to-catechol group ratio. Further, cell association was reduced by a factor of 2.5 by employing 20 kDa 8-arm PEG instead of 2.5 kDa 2-arm PEG during film assembly. These results demonstrate that the applied macromolecular conjugation approach can be used to customize particle properties, potentially facilitating applications in therapeutic delivery, imaging, separations, and catalysis.

## INTRODUCTION

In recent years, advancements in both macromolecular and small molecule synthesis have led to substantial progress in the engineering of particles with a range of tailorable properties. The breadth of particles that has been investigated and applied includes hollow capsules,[1,2] functional inorganic particles,[3] self-assembled polymer micelles,[4,5] and biofunctional assemblies.[6,7] Applications of such particles span a wide array of areas, including biomedical imaging,[8] therapeutic delivery,[9–16] catalysis,[17] and environmental remediation.[18,19] Advances in coating and thin film technologies have further enabled the optimization of particle surface and interfacial properties for specific applications.[20,21] One such strategy for engineering particle coatings is via the assembly of supramolecular networks such as metal–phenolic networks (MPNs).[1,2] This robust and modular coating method is based on the coordination chemistry between metal ions and naturally occurring phenolic molecules that contain catechol and galloyl groups (e.g., tannic acid (TA))[1] and enables the deposition of MPN films on a broad range of substrates, from macroscopic supports to synthetic particles and biological cells.[1,2] The selection of specific phenolic molecules and metal ions for the network formation determines the mechanical properties, disassembly behavior, and functionality of the MPN films (or capsules when assembled on sacrificial particles).[8,22] Broadening the range of phenolic compounds and metal ions that can be used in the assembly process would extend the range of properties exhibited by MPN films/capsules. However, this approach is hindered by several factors. Firstly, the choice of metal ions is finite and inherently dependent on available ions. Secondly, the number and distribution of functional groups in commercially available phenolic compounds, such as TA, dopamine, gallic acid, and pyrocatechol, is also somewhat restrictive. Thirdly, the more complex and potentially more useful phenolic compounds found in nature (e.g., gallocatechins) are often too challenging or costly to

isolate and characterize in workable quantities. As such, there is a strong motivation to prepare well-defined and functional phenolic building blocks that could provide functional and structural diversity into the suite of MPN structures, and thus expand their range of accessible properties. One such solution to this is to prepare well-defined macromolecular phenolic building blocks. This necessitates the development of high-yielding, robust modification strategies that can enable quantitative incorporation of catechol groups into polymers.

Poly(ethylene glycol) (PEG) is a well-known highly biocompatible and stealth polymer with antifouling properties and high water solubility owing to steric repulsion and surface hydration.[23–25] Inspired by the intrinsic properties of PEG and phenolic compounds (i.e., the ability to coordinate with $Fe^{3+}$ and to adhere to diverse surfaces), catechol-functionalized PEG building blocks have been synthesized and applied to fabricate various biofunctional materials. For example, we previously reported the preparation of low-fouling MPN capsules using dopamine-conjugated 8-arm PEG.[26] Other reported examples include a pH-dependent, self-healing hydrogel composed of catechol-functionalized 4-arm PEG and $Fe^{3+}$ ions,[27] as well as a series of catechol-functionalized PEG-based block copolymers, which provided significant antifouling capacity for target surfaces.[28] These studies typically employ dopamine, dopamine analogues or dopamine derivatives in the functionalization procedure.[26–28] There are, of course, alternative phenolic molecules that can be used to incorporate catechol functionality to macromolecules, although these are often overlooked in favor of the well-characterized dopamine and its derivatives. One such molecule is caffeic acid, which includes a carboxylic acid moiety that could potentially be linked to an amine-functional polymer via amide formation, thus affording a polymeric caffeamide. Such an approach could provide a convenient alternative for synthesizing well-defined PEG-based phenolic macromolecules that could in turn be applied to MPN formation. Further, the

development of robust, quantitative modification approaches will enable the systematic study of how the macromolecular architecture (number of arms) and size (molecular weights) of the macromolecular constituent (PEG) can be used to tune the properties of an assembled MPN. In the absence of a quantitative and versatile conjugation technique, such studies are difficult to reliably conduct. Finally, the development of a modular modification strategy based on caffeic acid would enable conjugation of catechol groups not only to PEG, but more generally to other polymers incorporating pendent or terminal amine groups.

Herein, we designed and synthesized six different catechol-functionalized PEG building blocks (PEG-caffeamides) with different architectures and molecular weights: α,ω-bisfunctional PEG, referred to as 2-arm PEG-CAF (2.5 and 5 kDa), 4-arm PEG-CAF (5 and 10 kDa), and 8-arm PEG-CAF (10 and 20 kDa) (Scheme 1b). Specifically, we developed a synthetic strategy for polymer–catechol conjugation using the acyl-protected and activated intermediate, caffeic acid carbonic anhydride, which was coupled with high specificity (~95%) and yield (~90%) to end-functional PEG-amines, thus affording a series of catechol-functionalized PEG building blocks. The applied synthetic approach is shown to be a versatile and robust strategy to synthesize the macromolecular catechols. The synthesized PEG-caffeamides were subsequently examined as phenolic building blocks for the fabrication of PEG capsules with a range of tailorable properties via MPN assembly. In previous studies, we demonstrated the tuning of MPN capsule permeability (high,[29] moderate,[1] or low[30]) by controlling the coordination kinetics. We also demonstrated the control of permeability of MPN capsules through the choice of phenolic compounds, metal ions, and their ratio, which influenced the intermolecular dynamics and network formation.[31] In the present study, we focused on the effect of employing bespoke PEG-caffeamide building blocks to fabricate a range of MPN capsules with tailorable properties. Specifically, by varying the architecture and

molecular weight of the PEG-caffeamide building blocks, the shell thickness, permeability, and cell association behavior of the capsules could be tuned. Further engineering of the MPN capsule properties was demonstrated by selecting different sacrificial templates, namely carboxylic acid-functionalized polystyrene (PS-COOH, nonporous) and $CaCO_3$ (highly porous) particles. Using the reported conjugation chemistry to yield high-purity macromolecular phenolic building blocks, this study presents a straightforward and highly versatile approach for tailoring the properties of MPN capsules and potentially opens up further opportunities for the synthesis of MPN composite materials.

## EXPERIMENTAL SECTION

**Synthesis of Multi-Arm PEG-Caffeamides.** As a representative example, the synthesis of PEG-caffeamide building block using 2.5 kDa 2-arm PEG is described. Typically, 2-arm PEG-$NH_2$, $[PEG_{30}\text{-}NH_2]_2$, (2.6 kDa, 271 mg, $1.04 \times 10^{-4}$ mol, Sigma-Aldrich) was weighed into a 4 mL vial. Dry dichloromethane (DCM; 2.5 mL) was then added via a rubber septum, and the solution was stirred under nitrogen for several minutes. In a separate vial, iBoc-protected caffeic acid-carbonic anhydride (i-Boc caffeic acid, iBocCAF) was added (200 mg, $4.16 \times 10^{-4}$ mol) followed by dry DCM (2.0 mL). The solution was stirred under a gentle stream of nitrogen and cooled in an ice bath. The solution of $[PEG_{30}\text{-}NH_2]_2$ was then taken up into a syringe and slowly added dropwise to the solution of iBocCAF. After addition was complete, the solution was allowed to react (stirring) over ice and nitrogen for 1 h and then allowed to equilibrate to ambient temperature for 15 min. The solution was then concentrated to half its original volume and then added dropwise to excess cold diethyl ether to precipitate the product, $[PEG_{32}\text{-iBoc-caffeamide}]_2$ as a sticky clear residue. Precipitation was carried out twice to remove excess iBocCAF (mass yield: ~90%, % purity of end groups = 95%). Refer to Figure S12 for peak assignments.

$[PEG_{32}$-iBoc-caffeamide$]_2$ from the previous step (250 mg, $7.1 \times 10^{-5}$ mol) was dissolved in dry DCM (1.30 mL) in a vial. In a separate vial, a 32% v/v solution of isopropyl amine was prepared in dry DCM (500 μL of isopropylamine in 1.06 mL DCM). The PEG-iBocCAF solution was then added dropwise to the stirring isopropylamine/DCM solution. The final concentration of isopropylamine in DCM was ~17% v/v or 2.1 M, which is approximately 20 equivalents of isopropylamine per isobutyl carbonate group. The solution was stirred for 16 h at ambient temperature. The darkened solution was then concentrated to half its original volume and added dropwise to excess cold diethyl ether to precipitate the product, $[PEG_{36}$-caffeamide$]_2$, as a sticky tan residue. The solid was then dissolved in 0.1 M HCl buffer and dialyzed against acidic water for 3 days. The product was then freeze dried to isolate the product as a powder (cream) (yield: ~90%). Refer to Figure S13 for peak assignments. The 2-arm PEG-CAF was used for capsule fabrication and further referred to as 2.5 kDa 2-arm PEG.

**Synthesis of PEG-Caffeamide–$Fe^{III}$ MPN Capsules from PS-COOH Templates.** A particle dispersion (100 μL) of PS-COOH (1.86 ± 0.03 μm, 50 mg $mL^{-1}$) was transferred into a 1.7 mL microcentrifuge tube and washed twice with water. To wash the PS-COOH particles, water (500 μL) was added. The suspension was mixed by vortexing and sonication for 1–2 min, after which the particles were pelleted by centrifugation (2000*g*, 2 min). The supernatant (500 μL) was then discarded, and the process was repeated for a second wash. The PEG-caffeamide stock solution and $FeCl_3 \cdot 6H_2O$ solution were added to obtain final concentrations of 0.5 mM and 1–4 mM (1 mM for 2-arm PEG-CAF, 2 mM for 4-arm PEG-CAF, and 4 mM for 8-arm PEG-CAF), respectively, and mixed by vortexing for 2 min. The final concentration of the particles was 10 mg $mL^{-1}$. 3-(*N*-Morpholino)propanesulfonic acid buffer (25 mM, pH 7.4, 0.7 mL) was added to raise the pH to >7, leading to the formation of bis- and tris-coordination complexes between catechol

PEG and $Fe^{III}$. After increasing the pH, excess and unreacted materials were removed by pelleting the particles (2000*g*, 2 min) and the supernatant was discarded. The MPN-coated particles were washed three times with water (500 μL) by repeated centrifugation (2000*g*, 2 min). The particles were then resuspended in water (50 μL), and tetrahydrofuran (THF; 1 mL) was added to remove the PS-COOH templates. The MPN capsules were pelleted through centrifugation (2000*g*, 2 min) and washed with THF (500 μL) five times. At the final THF washing step, the capsules were pelleted through centrifugation (2000*g*, 3 min) and the supernatant was discarded. The resulting PEG-caffeamide–$Fe^{III}$ MPN capsules were washed with water once and resuspended in water (250 μL).

**Permeability Studies.** To assess the permeability of the PEG-caffeamide–$Fe^{III}$ MPN capsules, the dispersion of MPN capsules was mixed with an equal volume of fluorescein isothiocyanate-tagged dextran (FITC-dextran) solution (1 mg $mL^{-1}$) through pipetting onto a glass slide. After 5–10 min, confocal laser scanning microscopy (CLSM) images of the capsules were taken. Dark capsule interiors were considered to indicate the formation of an impermeable film, whereas capsules with interiors of similar fluorescence intensity to the outer environment were considered permeable. Around 50–100 capsules were examined. The permeability of the capsules was reported as a percentage of capsules permeable to FITC-dextran.

**Cell Association Experiments.** For flow cytometry analysis, RAW 264.7 cells were seeded in a 24-well plate at a $5 \times 10^4$ cells per well and then cultured in Dulbecco's Modified Eagle Medium (DMEM) with 10% fetal bovine serum (FBS) at 37 °C with 5% $CO_2$ for 20 h to allow cellular adhesion on the plates. The prepared fluorescent PEG-caffeamide–$Fe^{III}$ MPN capsules were added to the cells at a capsule-to-cell ratio of 50:1 and then incubated for 4 h to examine cell association. After incubation, the supernatant was discarded, and the cells were washed with Dulbecco's

phosphate-buffered saline (DPBS; 500 μL) three times. Trypsin solution (1×, 200 μL) was added to facilitate cell detachment, and the solution was maintained in the incubator (37 °C with 5% $CO_2$) for 5 min. For neutralization, DMEM solution (300 μL) was added and the detached cells were washed with DPBS (1 mL) three times through centrifugation (350*g*, 5 min, 4 °C). The cells were dispersed in DPBS (400 μL) and cell association was analyzed by flow cytometry. Relative fluorescence intensity (RFI) refers to the fluorescence intensity of treated cells relative to the fluorescence intensity of untreated cells.

For the CLSM analysis, RAW 264.7 cells were seeded into 8-well Lab-Tek chambered coverglass slides (Thermo Fisher Scientific, Waltham, MA, USA) at a cell density of $4 \times 10^4$ cells per well and then cultured in DMEM with 10% FBS at 37 °C with 5% $CO_2$ for 20 h to allow cellular adhesion on the plates. The prepared fluorescent PEG-caffeamide–$Fe^{III}$ MPN capsules were added to the cells at a capsule-to-cell ratio of 50:1 and then incubated for 4 h to evaluate cell association. After the incubation time had elapsed, the supernatant was discarded and the cells were washed with DPBS (400 μL) twice. Cells were fixed by adding 4% paraformaldehyde (200 μL) for 30 min at 37 °C, then washed with DPBS (400 μL) twice. The cell membranes were stained with wheat germ agglutinin–Alexa Fluor 594 conjugate (WGA594) for 5 min on ice, and the cell nucleus was dyed with Hoechst 33342 for 10 min at room temperature. CLSM imaging was performed to monitor the cell association of the capsules on a microscope equipped with a Plan Apo λ 60× 1.4 NA oil immersion objective, 405, 488, and 561 nm lasers, and 450/50, 525/50, and 595/50 bandpass emission filters. The images were processed by Fiji software.

**Cytotoxicity Studies of PEG-Caffeamide–$Fe^{III}$ MPN Capsules.** A 2,3-bis[2-methoxy-4-nitro-5-sulfophenyl]-2*H*-tetrazolium-5-carboxyanilide inner salt (XTT) assay was performed to examine the cytotoxicity of the capsules. RAW 264.7 cells were seeded on a 96-well plate at a

density of 8000 cells per well and incubated overnight. The culture media was then removed and replaced with either fresh media (for the cell control) or fresh media containing fluorescent PEG-caffeamide–$Fe^{III}$ MPN capsules at a particle-to-cell ratio of 100:1 for 24 or 48 h. After the treatment, the media was replaced with fresh media containing activated XTT (9 mL of 0.2 mg $mL^{-1}$ XTT in DMEM with 10% FBS was activated by adding 22.5 μL of 0.6 mg $mL^{-1}$ phenazine methosulfate in DPBS), and cells were further incubated for 3 h. Finally, cells were screened on an Infinite M200 microplate reader (Tecan, Switzerland). Absorbance readings were measured at 475 nm with 30 s shaking, and a reference wavelength of 675 nm was used. Cell viability was expressed as a percentage by normalizing the absorbance to that obtained for untreated cells. All experiments were performed in triplicate, and data are presented as the mean ± standard deviation (SD).

## RESULTS AND DISCUSSION

**Design and Synthesis of PEG-Caffeamides.** Direct amidation or esterification of phenolic carboxylic acid small molecules can be conducted without the implementation of protective strategies for phenolic hydroxyl groups.[32–34] However, with such an approach, the yields can be diminished by side reactions, such as the self-condensation of phenol hydroxyl and carboxylic acid groups.[35–38] Reasonable conversions (>60%) to the desired esters or amides are more likely guaranteed using successive steps, namely (1) protection (of the phenolic hydroxyl group); (2) activation of the carboxylic acid group (for example using coupling agents such as 1-hydroxbenzotriaxole, *N,N′*-dicyclohexylcarbodiimide, or acid chlorides); (3) condensation with alcohol or amine; and finally (4) deprotection.[39,40] A range of protective groups and conjugation chemistries have been applied to yield libraries of phenolic acid esters and amide derivatives such

as caffeates and caffeamides. These have been shown to possess important properties such as anti-inflammatory, antioxidant, antitumor, and antibacterial activity.[41]

**Scheme 1. (a) Structures and Molecular Weights of End-Functional PEG-Amine Precursors. (b) Synthesis of 2-, 4-, and 8-Arm PEG-CAF Building Blocks Using the Caffeic Acid Carbonic Anhydride Method: (i) isoButyl Chloroformate, *N*-Methyl Morpholine, and Triethylamine in THF at −15 °C; (ii) 0 °C, DCM, 1 h; and (iii) Isopropyl Amine in Excess, DCM, Room Temperature.**

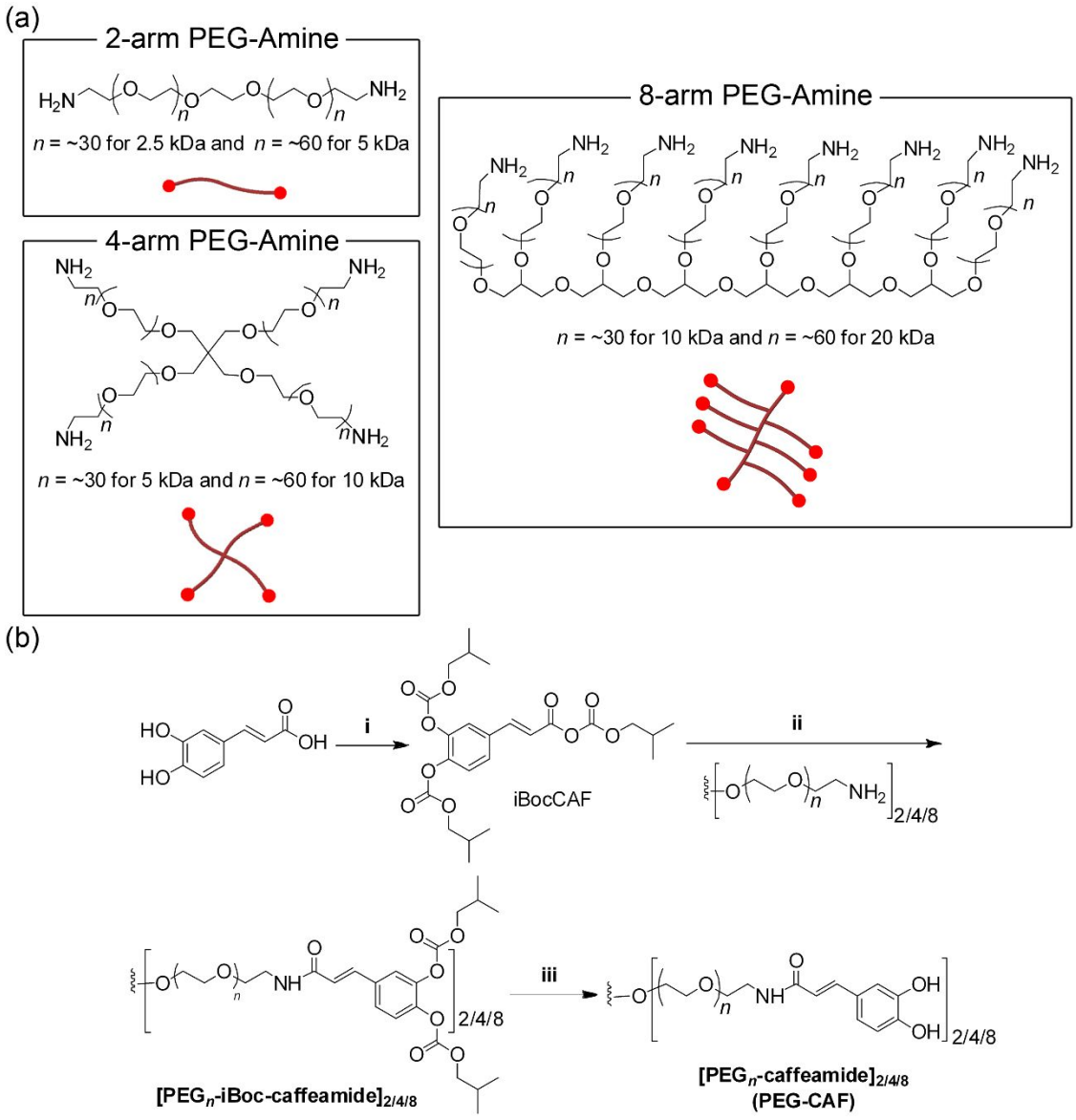

Using mixed carboxylic-carbonic anhydrides, which are activated forms of carboxylic acids, has proven successful for the formation of amide bonds, particularly for peptide linkages,[42–44] and this approach has also been applied to the synthesis of low molecular weight caffeates and caffeamides.[45] Using an alkyl chloroformate, simultaneous protection (of hydroxyls) and activation (of the carboxylic acid group) can be conducted to yield the protected and activated caffeic acid-carbonic anhydride. Subsequent reaction of the carboxylic-carbonic anhydride with an alcohol or amine then affords the corresponding ester or amide, with deprotection facilitated using an excess of amine. In this work, caffeic acid-carbonic anhydride was used to synthesize a series of PEG-caffeamide building blocks with different molecular weights and architectures by conjugating to a range of end-functional PEG-amine molecules as starting materials (Scheme 1). The synthesis of iBocCAF (Scheme 1b) was performed in one step using isobutyl chloroformate, *N*-methyl morpholine, and triethylamine. Both hydroxyls in caffeic acid are protected as isobutyl carbonate groups, while the carboxylic acid is activated as the carbonic anhydride. Amide bond coupling between iBocCAF and the PEG-amine was then performed in DCM for 1 h by mixing the two solutions while cooling to afford a series of protected caffeamide-functionalized PEG building blocks, $[PEG_n\text{-iBoc-caffeamide}]_m$, where $m$ is 2, 4, or 8. In this step, amide bond formation occurs via reaction of the amine with the caffeic acid carbonyl, with a loss of $CO_2$ and isobutanol (Scheme S1). The protected PEG-caffeamide building blocks ($[PEG_n\text{-iBoc-caffeamide}]_{2/4/8}$) were isolated by precipitation and analyzed before deprotection (see Figures S1–S26 for synthetic details and analysis of the end-functional PEG-amine, and protected and isolated PEG-caffeamide building blocks). In the case of small molecules, a one-pot conjugation followed by deprotection is typically conducted.[42,45–47] However, in the present work, we implemented a two-step strategy to monitor the formation of the carbamate side product. This is formed upon

reaction of the amine with carbonate groups during the coupling step, in this case yielding [iBoc-$PEG_n$ carbamate] arms (as shown in Scheme S2). This side reaction is known to occur during peptide synthesis and is thought to be influenced by the nature of the amine (i.e., primary or secondary), temperature, and solvent.[48] However, in the case of peptide coupling, racemization is an additional factor that needs to be considered. In our conjugation, the PEG carbamate product was not functionalized with catechols and could not be removed from the final product. Therefore, it was important to monitor the side product and identify conditions for minimizing its formation. A low molecular weight PEG-carbamate, i.e., [iBoc-$PEG_7$ carbamate]$_2$ was synthesized (Figure S9) to allow the identification and quantitation of the side product by $^1$H NMR spectroscopy. Using an excess of iBocCAF for coupling (1.5–2 equivalents vs. amine) was key to yielding minimal amounts of carbamate side product (~5% vs. the desired [$PEG_n$-iBoc-caffeamide]$_{2/4/8}$ product). In the next step, a low molecular weight amine (primary or secondary) was required to deprotect the carbonate groups—herein, we used isopropyl amine. A small molecule carbamate was thus formed upon deprotection via reaction of the small molecule amine with isobutyl carbonate groups. The carbamate was extracted from the polymer mixture by precipitation, and the polymer subsequently purified by dialysis. For each polymer, a large excess of amine was added to completely deprotect the isobutyl carbonate groups, yielding [$PEG_n$-caffeamide]$_{2/4/8}$ products in high purity and specificity. In the case of [$PEG_{60}$-caffeamide]$_4$, a small amount of unprotected arm remained in the mixture but this was deemed insignificant by $^1$H NMR analysis (<5%).

It is worth noting that a series of end-functional PEG-amine building blocks used in this study were synthesized in-house using commercially sourced hydroxyl end-functional PEG (see Figures S3–S8). Specifically, six end-functionalized PEG amine molecules with different structures and molecular weights were prepared: α,ω-bisfunctional 2-arm PEG-$NH_2$ (2.5 and 5 kDa), 4-arm PEG-

$NH_2$ (5 and 10 kDa), and 8-arm PEG-$NH_2$ (10 and 20 kDa) (structures displayed in Scheme 1a). As part of this procedure, the Staudinger reaction was used to produce iminophosphorane end groups from corresponding azides, which were then converted into the amines in situ.[49] This is by no means the only methodology for introducing amine functionality to a polymer and ought not be construed as an exclusive and essential step in the caffeamide functionalization: an alternative amination approach could equally be used. Further, while conversion of the iminophosphorane end groups into amines is commonly achieved via hydrolysis in water, methanolysis can be used as an alternative to hydrolysis to produce the amine. Methanolysis was applied in the current study, owing to the ease of reagent removal. We note that the application of methanolysis results in a small amount of methylated amine end groups (secondary and tertiary) in addition to the primary amine. This was particularly evident for the 2-arm PEG-$NH_2$ (2.5 and 5 kDa, Figures S3 and S4). Therefore, the converted [PEG$_n$-iBoc-caffeamide]$_{2/4/8}$ products also showed some small methyl peaks in their $^1$H NMR spectra (3.0–3.3 ppm in Figures S10, S11, S15, and S16). Commercial PEG amines were therefore substituted as starting materials to generate the 2-arm PEG-CAF products ([PEG$_n$-caffeamide]$_2$) and accordingly their $^1$H NMR spectra did not feature such peaks. Nevertheless, this factor had no apparent effect on subsequent capsule properties, and further optimization of amine synthesis was therefore not pursued. It is also important to note that amine functionality might be incorporated into the polymer via chemistries other than the Staudinger reaction, or, as noted above, commercially available polymeric amines might be used as the substrate for functionalization. Moreover, although we have exemplified the approach here using a PEG-amine library, it is important to note that functionalization via iBocCAF is equally applicable to other amine functional polymers.

The resulting [PEG$_n$-caffeamide]$_{2/4/8}$ polymers with different architectures (2-, 4-, and 8-arms) and molecular weights were used as MPN building blocks for the capsule studies and referred to as: 2.5 kDa 2-arm PEG-CAF, 5 kDa 2-arm PEG-CAF, 5 kDa 4-arm PEG-CAF, 10 kDa 4-arm PEG-CAF, and 10 kDa 8-arm PEG-CAF and 20 kDa 8-arm PEG-CAF, as outlined in Table S1.

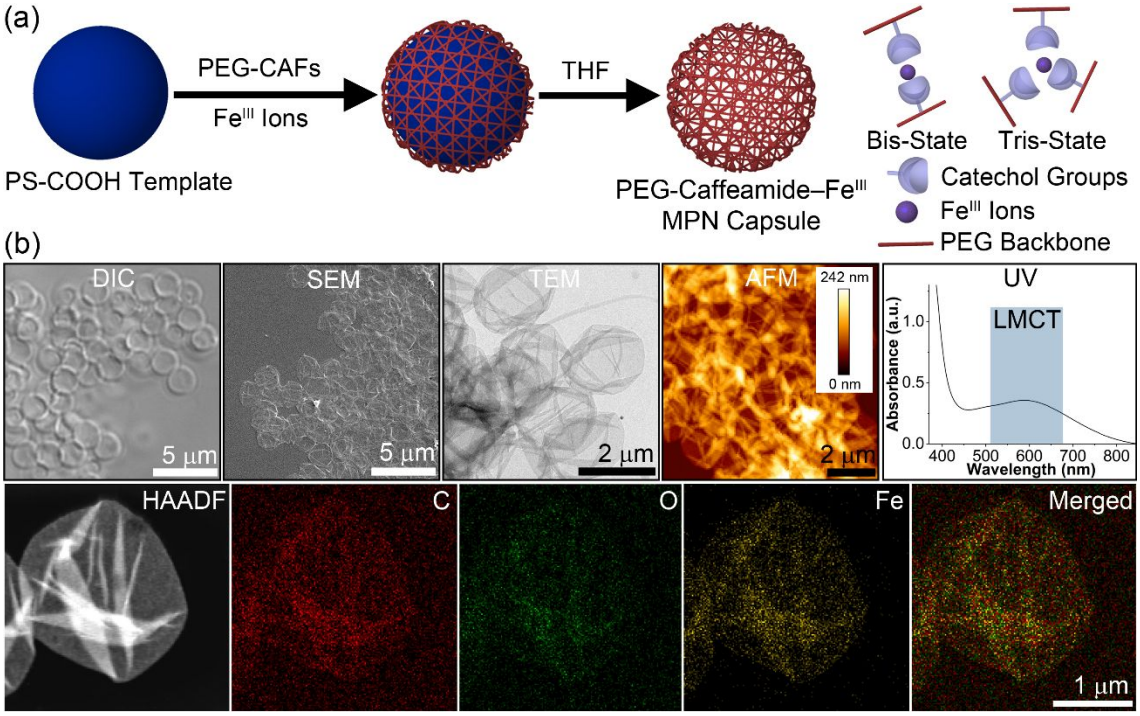


**Figure 1.** (a) Schematic of the preparation of PEG-caffeamide–Fe$^{III}$ MPN capsules using PS-COOH templates. (b) Characterization of PEG-caffeamide–Fe$^{III}$ MPN capsules (using 10 kDa 4-arm PEG-CAF) derived from PS-COOH sacrificial particles using DIC, SEM, TEM, AFM, UV–vis spectroscopy, HAADF, and EDX elemental mapping. The UV–vis absorption spectrum of the PEG-caffeamide–Fe$^{III}$ system shows an LMCT band, which indicates the formation of bis- and tris-state MPN complexes.

**Fabrication of PEG-Caffeamide–Fe$^{III}$ MPN Capsules.** MPN film formation via the coordination of PEG-caffeamide building blocks and Fe$^{III}$ ions was achieved on sacrificial template particles, namely, PS-COOH (1.86 ± 0.03 μm) particles (Figure 1a and S27a). PEG-

caffeamide solutions and $FeCl_3 \cdot 6H_2O$ were successively added to the suspension of sacrificial particles, followed by the addition of buffer solution (pH 7.4) to increase the pH of the suspension. The change in pH resulted in the cross-linking of the PEG-caffeamide–$Fe^{III}$ MPNs based on the formation of bis- and tris- coordination states. MPN capsules were obtained following dissolution of the PS-COOH template particles in THF. The coordination between the $Fe^{III}$ ions and PEG-caffeamide building blocks in the MPN capsules was characterized by UV–vis spectroscopy analysis. This coordination exhibited the pH-dependent transitions expected between mono-, bis-, and tris-complex states (Figure S28). A characteristic ligand-to-metal charge transfer (LMCT) band was detected around 565 nm, indicating bis- and tris-type coordination between $Fe^{III}$ and PEG-caffeamide, where the bis-state was dominant, in the capsules (Figures 1b and S28).[1,50] The preparation of MPN capsules composed of natural phenolic compounds (e.g. TA, gallic acid, pyrogallol, and pyrocatechol) and $Fe^{III}$ ions was previously reported using PS particles as sacrificial templates.[1,22] In the present work, the PEG-caffeamide–$Fe^{III}$ MPN films (using PEG-caffeamide building blocks) were successfully deposited on carboxylic acid-functionalized PS particles instead of bare PS particles via hydrogen bonding between the PEG backbone and carboxylic acid groups, which appears to be a key factor for MPN film deposition (Figure S29).

As a representative sample, the characterization of PEG-caffeamide–$Fe^{III}$ MPN capsules prepared from PS-COOH templates using 10 kDa 4-arm PEG-CAF and $Fe^{III}$ is shown in Figure 1b. The capsules were well dispersed in aqueous solution, as observed from the differential interference contrast (DIC) microscopy image in Figure 1b. Scanning electron microscopy (SEM), transmission electron microscopy (TEM), atomic force microscopy (AFM), and high-angle annular dark-field (HAADF) microscopy revealed collapsed capsule structures with folds and creases, which are characteristic of collapsed capsules following drying in air. Energy-dispersive

X-ray spectroscopy (EDX) elemental mapping revealed that C, O, and Fe were all uniformly distributed throughout the PEG-caffeamide–$Fe^{III}$ MPN capsules. Fourier transform infrared spectroscopy additionally confirmed the presence of PEG in the resulting capsules (Figure S30).

A different MPN capsule system (Figure S31) was additionally fabricated using 10 kDa 4-arm PEG-CAF and porous $CaCO_3$ particles (3.19 ± 0.34 μm) as sacrificial templates (Figure S27b). The templates were selectively dissolved using ethylenediaminetetraacetic acid (EDTA). The AFM data showed that the overall shell thickness of the capsules prepared using $CaCO_3$ templates were thicker (163 nm vs 16 nm) than the PS-COOH-templated capsules (Figure 1b, Figure S31, and Table S2). Coordination between catechol-PEG and $Fe^{III}$ has been reported to occur within the highly porous $CaCO_3$ particles,[12] generating thicker shells. Overall, these results demonstrate that well-defined capsules can be prepared via MPN formation between the synthesized PEG-caffeamides and $Fe^{III}$ ions.

**Scheme 2. PEG-Caffeamide–$Fe^{III}$ MPN Capsules Prepared from Coordination-Driven Cross-Linking of $Fe^{III}$ Ions with Different 2-, 4-, or 8-arm PEG-CAF Building Blocks Using PS-COOH Templates.**

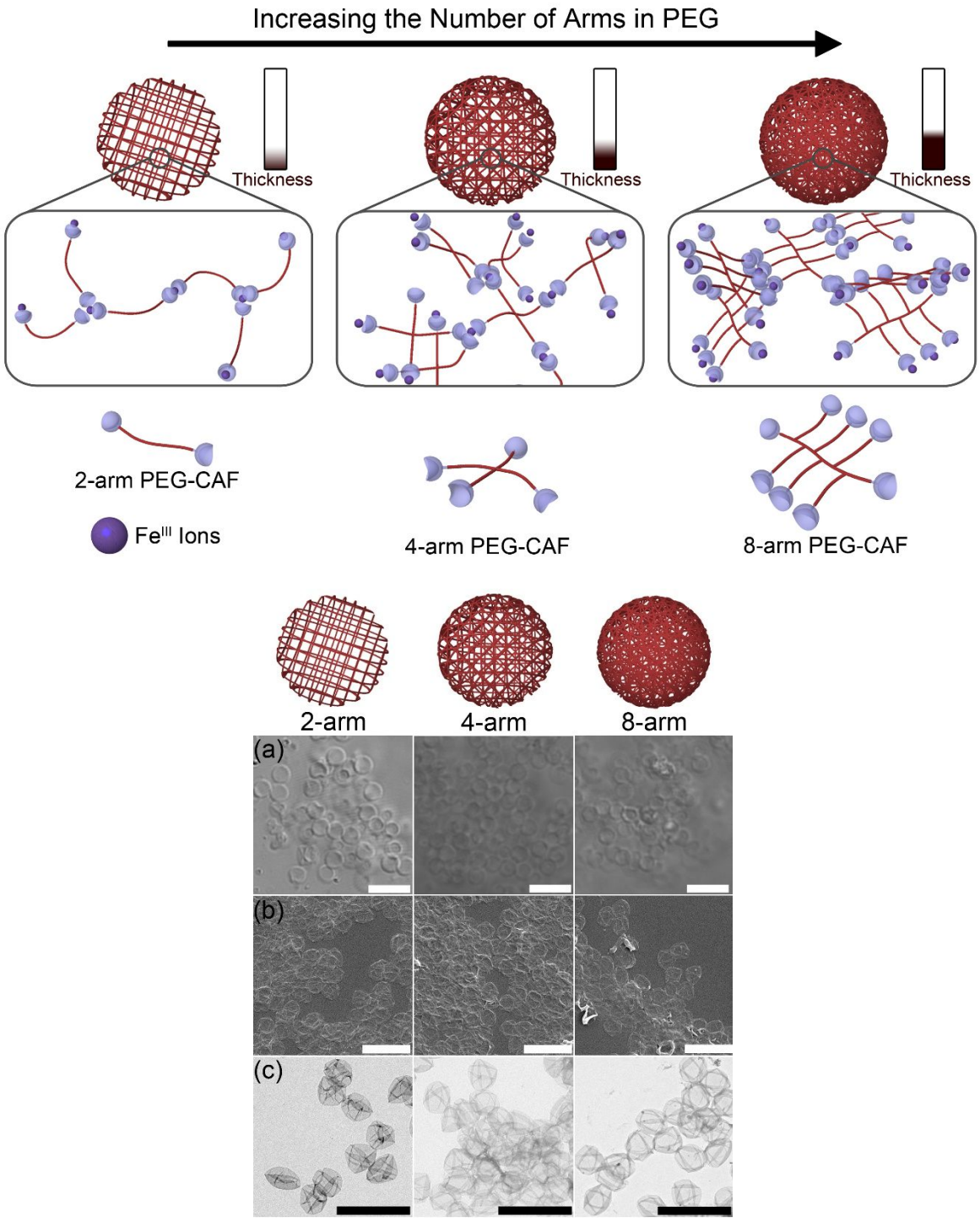


**Figure 2.** Microscopy images of PEG-caffeamide–$Fe^{III}$ MPN capsules prepared from 2.5 kDa 2-arm, 5 kDa 4-arm, and 10 kDa 8-arm PEG-CAFs and PS-COOH templates: (a) DIC, (b) SEM, and (c) TEM images. All scale bars are 5 μm.

**Engineering the Shell Thickness of MPN Capsules.** The conventional MPN film formation, which occurs via a discrete assembly process, generally creates hollow capsules with a film thickness of approximately 10 nm regardless of the metal ion, phenolic building block, or phenolic compound-to-metal molar ratio selected.[1,8,22] Additionally, it is difficult to control the film thickness owing to rapid film growth (<1 min) using these parameters.[1,30] Using alternative approaches, i.e., by repeating the MPN coating cycle[12] or via continuous assembly,[51] MPN capsules with different shell thicknesses can be engineered. However, these methods require repetitive and multiple steps or longer times for film formation (~4 h). In contrast, in the present work, we postulated that a simple and more rapid methodology (<2 min), involving only one discrete deposition step, could be used to tune the shell thickness of the capsules by varying both the architecture (2-, 4-, and 8-arm) and the molecular weight ($M_n$ 2.5–20 kDa) of the PEG-caffeamide building blocks prepared herein (Scheme 2). To investigate this approach, six types of PEG-caffeamide–$Fe^{III}$ MPN capsules were first fabricated from PS-COOH sacrificial templates and using the six PEG-caffeamide building blocks (2-arm PEG-CAF (2.5 and 5 kDa), 4-arm PEG-CAF (5 and 10 kDa), and 8-arm PEG-CAF (10 and 20 kDa)). The capsules were characterized via DIC, SEM, TEM, and dynamic light scattering (DLS) (Figures 2, S32, and S33a). As observed from the DIC images and DLS analysis, the PEG-caffeamide–$Fe^{III}$ MPN capsules were stable and monodisperse. Moreover, SEM and TEM images revealed the typical surface morphology of collapsed capsules.

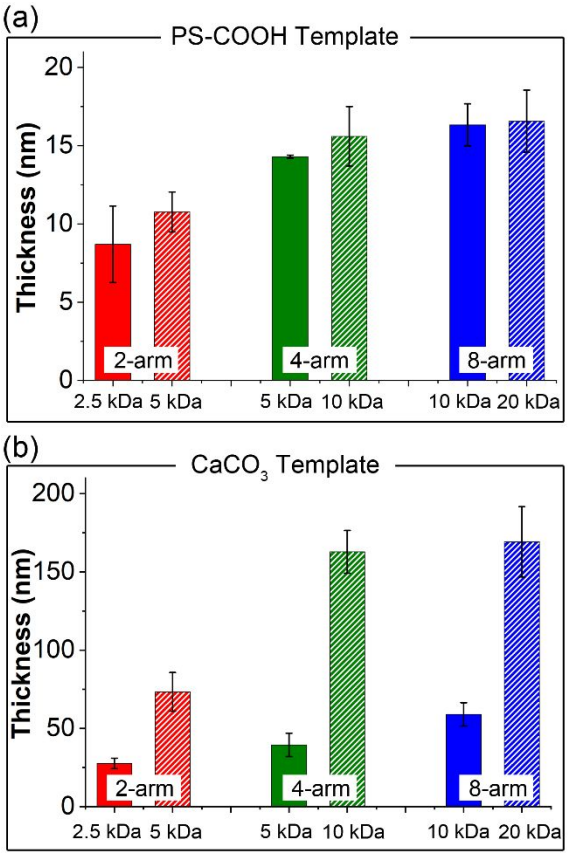


**Figure 3.** Comparison of the shell thickness of PEG-caffeamide–$Fe^{III}$ MPN capsules prepared from (a) PS-COOH templates and (b) $CaCO_3$ templates and various PEG-caffeamide building blocks: 2.5 kDa 2-arm and 5 kDa 2-arm; 5 kDa 4-arm and 10 kDa 4-arm; and 10 kDa 8-arm and 20 kDa 8-arm. The PEG-to-catechol ratios were 1250:1 (solid bars) and 2500:1 (diagonal stripes). The thickness was determined by height–distance AFM graphs and the data are shown as the mean ± SD of three independent AFM measurements. Scale bars are 5 μm.

Subsequently, we explored assembly of the same six polymers using porous $CaCO_3$ particles as the template. In this case, PEG-caffeamide–$Fe^{III}$ MPN film deposition occurs within the porous structures of the particles[12] (Scheme S3). The obtained capsules were characterized by DIC, SEM, TEM, and DLS (Figures S33b and S34). The $CaCO_3$-templated MPN capsules exhibited fewer folds and creases than the PS-COOH-templated MPN capsules, suggesting thicker capsule walls

(see below for a quantitative discussion). Overall, these results indicate that variation of the template has a significant effect on shell properties.

To provide a quantitative comparison of the shell thickness of the capsules, the PEG-caffeamide–$Fe^{III}$ MPN capsules were examined by AFM (Figures 3, S35, and S36). The thickness of the PS-COOH-templated MPN capsules showed a dependency on the type of the PEG-caffeamide building block used (which is detailed in subsequent discussion). A thin film layer ranging from 8.7 to 16.6 nm was observed (Figures 3 and S35 and Table S2). This thickness range is comparable with the shell thickness typically observed for conventionally prepared TA–$Fe^{III}$ MPN capsules (~10 nm).[1] In contrast, the $CaCO_3$-templated PEG-caffeamide–$Fe^{III}$ MPN capsules displayed thicker shells with a broad range of attainable thickness (27.6–169.3 nm) (Figures 3 and S36 and Table S2), further confirming that the sacrificial template greatly influences the thickness of the capsules. The shell thickness was also affected by the concentration of PEG-caffeamide in the assembly solution (Figure S37a). Specifically, PEG-caffeamide–$Fe^{III}$ MPN capsules prepared using 0.25 mM 10 kDa 4-arm PEG-caffeamide have thinner shells than capsules prepared using 0.5 and 1 mM 10 kDa 4-arm PEG-caffeamide. Further, incubating the template particles for different times in the assembly solution (i.e., 2, 20, and 60 min) led to similar shell thicknesses (Figure S37b).

Regardless of the particle template employed, the shell thickness was largely dependent on the structure and $M_n$ of the PEG-caffeamide building blocks. One primary factor affecting shell thickness is the polymer structure itself. Across the range of PS-COOH-templated capsules prepared, the increase in shell thickness correlated with an increase in the number of arms in the PEG-caffeamide building blocks (Figure 3a). During the deposition process, network formation is facilitated by the coordination of the $Fe^{III}$ ions with the catechol end groups, which leads to

bridging between individual polymer chains. A higher number of PEG arms thus corresponds to a higher number of catechol end groups and therefore the concurrent formation of more interconnections. Overall, this results in enhanced polymer deposition and therefore the formation of thicker films. Maintaining the same number of PEG arms (and therefore number of catechol end groups) while increasing the $M_n$ of PEG also resulted in thicker capsule films (Figure 3a). This trend can be attributed to hydrogen bonding interactions between the polymer chains in the network, as well as with water and the template itself. The hydrogen bonding interactions are more significant in films with a higher proportion of PEG. It is notable that for the PS-COOH-templated capsules, the increase in shell thickness while increasing PEG $M_n$ at a given PEG arm number is not significant. However, in the case of the $CaCO_3$-templated capsules, the effect of the PEG $M_n$ (at a given PEG arm number) on the shell thickness was more pronounced. This was particularly evident for the 4-arm PEG capsules, where the capsules prepared from 10 kDa PEG-CAF were approximately 4× thicker than the capsules prepared from 5 kDa PEG-CAF (Figure 3b). To better understand the thickness trend obtained, the PEG $M_n$-to-catechol (end group) ratio was examined, as this determines both the concentration of anchor points in the final network and the length of the PEG chain that separates each anchor point. Within the PEG-caffeamide building block series, two groups were distinguished based on the PEG $M_n$-to-catechol ratio (1250:1 and 2500:1 groups, refer to Table S1). The higher ratio group (2500:1) had a higher $M_n$ PEG chain separating each catechol–$Fe^{III}$ anchor point, and this group consistently displayed higher thickness values across the PEG-arm series (Figure 3), likely due to hydrogen bonding interactions that significantly affected film growth.

For the $CaCO_3$-templated particles, a different trend was observed from that observed for the PS-COOH-templated capsules. The thickness of the capsules formed using the 5 kDa 2-arm PEG-

CAF was larger than that for the capsules formed from the corresponding 5 kDa 4-arm PEG-CAF. The same effect was evident for the 10 kDa 4-arm PEG-CAF capsules, which were thicker than the 10 kDa 8-arm PEG-CAF capsules. In these cases, at a given PEG $M_n$, a significantly thicker capsule wall was formed using fewer arms (i.e., less catechol end groups). The greater number of anchor points available for complexation is likely to result in larger aggregates being formed more rapidly, thus restricting diffusion of the polymer into the pores of the $CaCO_3$.

Overall, we demonstrate a rapid and straightforward methodology for tuning film thickness of PEG-caffeamide–$Fe^{III}$ MPN capsules via AFM analysis. By changing the properties of PEG (i.e. architectures and molecular weights), combined with the type of sacrificial particles (porous or nonporous), large adjustments in capsule shell thickness can be engineered, ranging from 8.7 to 169.3 nm. In the case of PS-COOH templated capsules, which have thinner walls overall compared with the $CaCO_3$-templated capsules, minor increases in capsule thickness were achieved by increasing the proportion of PEG in the PEG-caffeamide building block. This was facilitated by either increasing the number of arms or the $M_n$ of PEG itself. For the $CaCO_3$-templated capsules, thicker walls were formed due to infiltration of the network into the porous structure of the template. However, by simply increasing the number of catechol end groups in the building blocks, which form the anchor points in the network, a reduction in film thickness was achieved due to likely reduced diffusion of the $Fe^{III}$-complexed polymer chains into the pores of the $CaCO_3$ template.

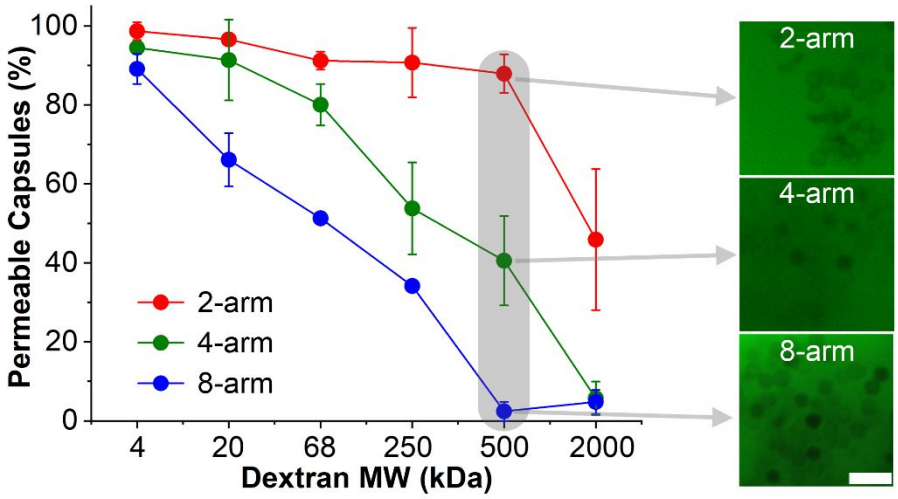


**Figure 4.** Comparison of the permeability of PEG-caffeamide–$Fe^{III}$ MPN capsules prepared using PS-COOH templates and 2.5 kDa 2-arm, 5 kDa 4-arm, and 10 kDa 8-arm PEG-CAF against FITC-dextran with molecular weight (MW) ranging from 4 to 2000 kDa. The PEG $M_n$-to-catechol ratio was 1250:1. Scale bars are 5 μm. Error bars represent the SD of three independent experiments.

**Modulating Film Permeability.** Capsule properties such as stiffness, permeability, and cell association behavior are influenced by the capsule shell thickness.[12,51,52] As the thickness of the capsule wall was influenced by the structure and composition of the PEG-caffeamide building block, we investigated whether the permeability of the PEG-caffeamide–$Fe^{III}$ MPN capsules could be controlled in an analogous manner. The permeability of the PEG-caffeamide–$Fe^{III}$ MPN capsules was probed by incubating the capsules with FITC-dextran of different molecular weights, ranging from 4 to 2000 kDa (Figures 4, S38–S41). As observed, the PS-COOH-templated MPN capsules, prepared from different PEG-caffeamide building blocks, displayed variable permeability against FITC-dextran molecules (Figures 4, S38, and S39). The permeability of the PEG-caffeamide–$Fe^{III}$ MPN capsules prepared from 2-arm, 4-arm, or 8-arm PEG-CAFs with a PEG $M_n$-to-catechol ratio of 1250:1 was examined. Increasing the number of arms (and therefore

number of catechols) resulted in a reduction in permeability. Specifically, 87.9% of 2-arm PEG-caffeamide–$Fe^{III}$ MPN capsules (regarded as highly permeable), 40.6% of 4-arm PEG-caffeamide–$Fe^{III}$ MPN capsules (regarded as moderately permeable), and 2.4% of 8-arm PEG-caffeamide–$Fe^{III}$ MPN capsules (regarded as nearly impermeable) were permeable to varying extents to 500 kDa FITC-dextran (Figures 4 and S39a). When a higher PEG-to-catechol ratio of 2500:1 was employed, the capsules followed a similar permeability trend, with similar levels achieved (Figure S38). Specifically, 89.1% of 2-arm PEG-caffeamide–$Fe^{III}$ MPN capsules (highly permeable), 45.8% of 4-arm PEG-caffeamide–$Fe^{III}$ MPN capsules (moderately permeable), and 19.6% of 8-arm PEG-caffeamide–$Fe^{III}$ MPN capsules (nearly impermeable) were permeable to varying degrees to 500 kDa FITC-dextran (Figures S38 and S39b). Higher permeability is associated with a less dense network structure, i.e., with a higher proportion of PEG and fewer $Fe^{III}$–catechol cross-links.[31] This was achieved using a PEG-caffeamide building block with fewer catechol-functionalized PEG arms (2 arm vs. 4 arm vs. 8 arm). The results correlate with the shell thickness trends, where a significant reduction in capsule thickness is obtained by reducing the number of arms, resulting in a network structure with fewer crosslinks (anchor points).

In contrast, the $CaCO_3$-templated PEG-caffeamide–$Fe^{III}$ MPN capsules showed significantly reduced permeability, with less than 25% of the 2-arm PEG-caffeamide–$Fe^{III}$ MPN capsules and close to 0% of the 4- and 8-arm PEG-caffeamide–$Fe^{III}$ MPN capsules being permeable to a range of FITC-dextrans (4–2000 kDa) (Figures S40 and S41). These results are likely due to the thicker shell layers formed on these capsules (ranging from 27.6 to 169.3 nm) (Figure 3b and Table S2). Interestingly, the PEG-caffeamide–$Fe^{III}$ MPN capsules prepared from 10 kDa 4-arm PEG-CAF and 20 kDa 8-arm PEG-CAF, which had the thickest shells (162.9 and 169.3 nm, respectively), were impermeable even to 4 kDa FITC dextran (Figure S40b), thus showing the robust and

impermeable feature of the shell. The low permeability achieved herein is lower than that reported for MPN capsules prepared from discrete assembly[1,31] or oxidation-mediated coordination assembly,[30] thus showing promise for loading small molecule drugs. These results demonstrate that with proper selection of the PEG building block and sacrificial template, the permeability of PEG-caffeamide–$Fe^{III}$ MPN capsules can be tuned from 0 to 100% over a wide molecular weight range (e.g., 4–2000 kDa dextran). The present methodology, which allows fine and broad tuning of capsule permeability, could potentially be employed for engineering capsules for various applications, including therapeutic delivery, sensing, separations, and catalysis.[12–16,30]

**Controlling Cell Association of PEG-Caffeamide–$Fe^{III}$ MPN Capsules.** PEG has attracted much interest in biomedical applications owing to the stealth effect derived from its excellent antifouling behavior and high biocompatibility.[23–25,28] For instance, to prolong the blood circulation time of drug delivery systems, their surfaces have commonly been modified with PEG chains, which results in reduced nonspecific interactions.[53] The PEG-caffeamide–$Fe^{III}$ MPN capsules are expected to have tunable stealth properties arising from the different architectures and molecular weights of the PEG building blocks used in the network system. To compare the stealth properties of the different PEG-caffeamide–$Fe^{III}$ MPN capsules, fluorescent MPN capsules were first prepared (Figure 5a). Briefly, fluorescent sacrificial template particles were prepared via physical interactions between $CaCO_3$ particles and 2000 kDa FITC-dextran. Capsules exhibiting green fluorescence were then obtained through successive MPN film deposition on the as-prepared FITC-dextran labeled $CaCO_3$ templates and template removal with EDTA. The FITC-dextran-labeled $CaCO_3$ particles and fluorescent PEG-caffeamide–$Fe^{III}$ MPN capsules were characterized by CLSM (Figure 5b). The observed fluorescent ring structures of the capsules likely derive from hydrogen bonding interactions between dextran and the PEG film. To investigate the stealth

properties of the fluorescent PEG-caffeamide–$Fe^{III}$ MPN capsules, their cell association profiles were analyzed by flow cytometry and CLSM to determine the green fluorescence intensity originating from the cell-associated fluorescent MPN capsules (Figure S42).

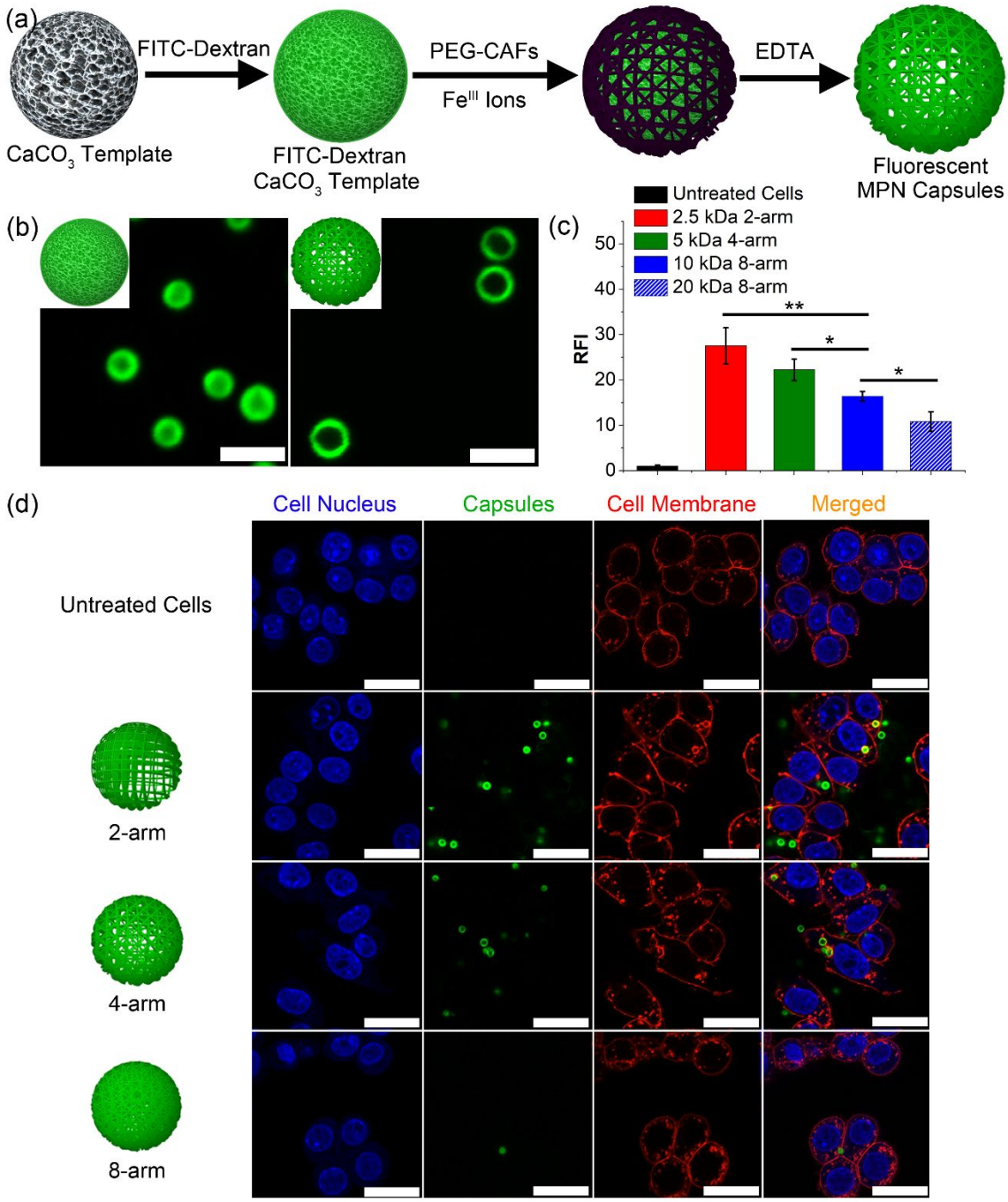

**Figure 5.** (a) Schematic illustration of the preparation of fluorescent MPN capsules using FITC-dextran-labeled $CaCO_3$ particles. (b) Fluorescence microscopy images of FITC-dextran (2000 kDa)-labeled $CaCO_3$ particles (left) and fluorescent PEG-caffeamide–$Fe^{III}$ MPN capsules (right). (c) Flow cytometry analysis of RAW 264.7 cells treated with fluorescent PEG-caffeamide–$Fe^{III}$ MPN capsules prepared from 2.5 kDa 2-arm, 5 kDa 4-arm, 10 kDa 8-arm, and 20 kDa 8-arm PEG-CAF building blocks, following incubation for 4 h at 37 °C. The PEG $M_n$-to-catechol ratios were 1250:1 (solid bars) and 2500:1 (diagonal stripes). RFI to untreated cells is shown. Error bars represent the SD of three independent experiments. Statistical significance was determined by one-way ANOVA analysis: ** $p < 0.01$ and * $p < 0.05$. (d) CLSM images of Raw 264.7 cells incubated with fluorescent PEG-caffeamide–$Fe^{III}$ MPN capsules prepared from 2.5 kDa 2-arm, 5 kDa 4-arm, and 10 kDa 8-arm PEG-CAF for 4 h at 37 °C. Cell membranes and nuclei were stained with WGA594 (red) and Hoechst 33342 (blue), respectively. Green fluorescence represents fluorescent MPN capsules. Scale bars are 5 μm (b) and 20 μm (d).

Capsules prepared from different PEG-caffeamide building blocks (2-, 4-, and 8-arm PEG-CAF with a PEG $M_n$-to-catechol ratio of 1250:1) were incubated with RAW 264.7 macrophage cells for 4 h at 37 °C at a capsule-to-cell ratio of 50:1. As observed in Figure 5c, the fluorescence intensity (relative to untreated cells) of RAW 264.7 cells treated with PEG-caffeamide–$Fe^{III}$ MPN capsules decreased from 27.5 to 22.2 and 16.4 RFI with increasing number of arms from 2 to 8 in the PEG building blocks. Moreover, the RFI decreased further to 10.8 RFI by increasing the molecular weight of 8-arm PEG-CAF from 10 to 20 kDa. For visualization of the cell–capsule interactions, the cell nucleus and membrane were stained by Hoechst 33342 (blue) and WGA594 (red), which do not overlap with the fluorescence from the MPN capsules (green). Consistent with the flow cytometry results, 2-arm PEG-caffeamide–$Fe^{III}$ MPN capsules associated more significantly with

cells in comparison with 8-arm PEG-CAF capsules, which associated less with cells (Figure 5d). Increasing the proportion of PEG in the building blocks (to 2500:1, Figure S43) showed a similar trend in the RFI of the cells, that is, PEG-caffeamide–$Fe^{III}$ capsules prepared from PEG building blocks with more arms were more stealthy. The cytotoxicity of the resulting capsules was evaluated via XTT assay. No detectable toxicity was observed across the range of particle concentrations tested (Figure S44). These results demonstrate that the biological properties of the MPN capsules can also be controlled via judicious selection of the PEG-CAF building block, with an increase in the proportion of PEG-CAF in the building block resulting in reduced nonspecific cell association. The proposed methodology could therefore be used to control the fouling properties of capsules with potential in the development of advanced delivery vehicles for drugs or therapeutic nucleic acids.[10,54]

## CONCLUSIONS

In this work, we have demonstrated a versatile and robust approach for conjugating caffeic acid to amine functional polymers, thereby yielding an array of macromolecular phenolic building blocks for MPN assembly. Specifically, by reacting caffeic acid with isobutyl chloroformate, we were able to activate the carboxylic acid to amine addition (as the carbonic anhydride) while simultaneously protecting the hydroxyls as isobutyl carbonate groups. The resulting iBoc-protected caffeic acid-carbonic anhydride could be conjugated quantitatively to PEG-amines and deprotected under mild conditions to reveal a series of PEG-caffeamides. Specifically, PEG-caffeamide building blocks with different architectures and molecular weights (2-arm PEG (2.5 and 5 kDa), 4-arm PEG (5 and 10 kDa), and 8-arm PEG (10 and 20 kDa)) were synthesized. Well-defined MPN capsules were subsequently fabricated using the various PEG-caffeamide building blocks on different sacrificial particles via the coordination of catechol-end groups with $Fe^{III}$ ions.

The resulting particles displayed tunable capsule properties (shell thickness, permeability, and cell association), dictated by the nature of the PEG-caffeamide building block. Independent of the template chosen (PS-COOH or $CaCO_3$), the increase in shell thickness of the capsules correlated with an increase in the number of arms. Increases in PEG $M_n$ also resulted in thicker capsule films, due to hydrogen bonding, although this increase was more significant in the $CaCO_3$-templated capsules. Furthermore, the use of nonporous PS-COOH template particles afforded thinner films, whereas the use of porous $CaCO_3$ particles led to thicker films. The permeability profiles of the capsules were controlled by varying the structure of the PEG-caffeamide building block, with a systematic increase obtained by using fewer catechol-functionalized arms, as consistent with shell thickness trends. In the case of the porous $CaCO_3$-templated capsules, where capsule walls were significantly thicker, the capsules were significantly less permeable. The degree of cell association of the $CaCO_3$-templated capsules decreased by increasing the number of arms in the PEG-caffeamide building blocks and decreased further by increasing the proportion of PEG in the formed shell structure. These results demonstrate that, by combining a high yielding and versatile polymer conjugation approach with the judicious choice of capsule template, it is possible to tune MPN capsule properties over a wide range. Such micrometer-sized capsules could be of potential interest for controlled vaccine and pulmonary delivery applications.[12–16] Moreover, given that the reported conjugation strategy is applicable to almost any amine-functional substrate, the reported approach should provide a platform to further the biological application of MPN capsules as delivery vehicles[10,12–16,30,54,55] and for surface coating technologies.[56]

## ASSOCIATED CONTENT

**Supporting Information**. Materials and instrumentation; synthesis of PEG-caffeamide building blocks, $CaCO_3$ particles, FITC-dextran-labeled $CaCO_3$ particles, and fluorescent MPN capsules; thickness comparison of MPN capsules; and NMR; DIC; SEM; TEM; permeability; cell association; cytotoxicity data; and MIRIBEL checklist for reporting research in bio–nano science. This material is available free of charge via the Internet at http://pubs.acs.org.

## AUTHOR INFORMATION

### Corresponding Author

*E-mail: john.f.quinn@monash.edu (J.F.Q.) and fcaruso@unimelb.edu.au (F.C.)

### Author Contributions

§C.-J. K. and F.E. contributed equally to this work. The manuscript was written through contributions of all authors. All authors have given approval to the final version of the manuscript.

### Notes

The authors declare no competing financial interest.

## ACKNOWLEDGMENT

This research was funded by the Australian Research Council through the Discovery Project (DP200100713) scheme. F.C. acknowledges the award of a National Health and Medical Research Council Senior Principal Research Fellowship (GNT1135806). J.F.Q. acknowledges receipt of a Future Fellowship (FT170100144) from the Australian Research Council. This work was performed in part at the Materials Characterisation and Fabrication Platform (MCFP) at The

University of Melbourne and the Victorian Node of the Australian National Fabrication Facility (ANFF). We thank Dr. Christina Cortez-Jugo and Dr. Matthew Faria for helpful discussion.

REFERENCES

(1) Ejima, H.; Richardson, J. J.; Liang, K.; Best, J. P.; van Koeverden, M. P.; Such, G. K.; Cui, J.; Caruso, F. One-Step Assembly of Coordination Complexes for Versatile Film and Particle Engineering. *Science* **2013**, *341*, 154–157.

(2) Guo, J.; Tardy, B. L.; Christofferson, A. J.; Dai, Y.; Richardson, J. J.; Zhu, W.; Hu, M.; Ju, Y.; Cui, J.; Dagastine, R. R. et al. Modular Assembly of Superstructures from Polyphenol-Functionalized Building Blocks. *Nat. Nanotechnol.* **2016**, *11*, 1105–1111.

(3) Mirkin, C. A.; Letsinger, R. L.; Mucic, R. C.; Storhoff, J. A DNA-Based Method for Rationally Assembling Nanoparticles into Macroscopic Materials. *Nature* **1996**, *382*, 607–609.

(4) Lu, Y.; Lin, J.; Wang, L.; Zhang, L.; Cai, C. Self-Assembly of Copolymer Micelles: Higher-Level Assembly for Constructing Hierarchical Structure. *Chem. Rev.* **2020**, *120*, 4111–4140.

(5) Chan, L. W.; Anahtar, M. N.; Ong, T. H.; Hern, K. E.; Kunz, R. R.; Bhatia, S. N. Engineering Synthetic Breath Biomarkers for Respiratory Disease. *Nat. Nanotechnol.* **2020**, *15*, 792–800.

(6) Kim, C.-J.; Park, J.-e.; Hu, X.; Albert, S. K.; Park, S.-J. Peptide-Driven Shape Control of Low-Dimensional DNA Nanostructures. *ACS Nano* **2020**, *14*, 2276–2284.

(7) Samanta, D.; Ebrahimi, S. B.; Kusmierz, C. D.; Cheng, H. F.; Mirkin, C. A. Protein Spherical Nucleic Acids for Live-Cell Chemical Analysis. *J. Am. Chem. Soc.* **2020**, *142*, 13350–13355.

(8) Guo, J.; Ping, Y.; Ejima, H.; Alt, K.; Meissner, M.; Richardson, J. J.; Yan, Y.; Peter, K.; Elverfeldt, D. v.; Hagemeyer, C. E. et al. Engineering Multifunctional Capsules through the Assembly of Metal-Phenolic Networks. *Angew. Chem., Int. Ed.* **2014**, *53*, 5546–5551.

(9) Wang, X.; Yan, J.-J.; Wang, L.; Pan, D.; Yang, R.; Xu, Y.; Sheng, J.; Huang, Q.; Zhao, H.; Yang, M. Rational Design of Polyphenol-Poloxamer Nanovesicles for Targeting Inflammatory Bowel Disease Therapy. *Chem. Mater.* **2018**, *30*, 4073–4080.

(10) Blum, A. P.; Kammeyer, J. K.; Rush, A. M.; Callmann, C. E.; Hahn, M. E.; Gianneschi, N. C. Stimuli-Responsive Nanomaterials for Biomedical Applications. *J. Am. Chem. Soc.* **2015**, *137*, 2140–2154.

(11) Cheng, L.; Wang, C.; Feng, L.; Yang, K.; Liu, Z. Functional Nanomaterials for Phototherapies of Cancer. *Chem. Rev.* **2014**, *114*, 10869–10939.

(12) Ju, Y.; Cortez-Jugo, C.; Chen, J.; Wang, T. Y.; Mitchell, A. J.; Tsantikos, E.; Bertleff-Zieschang, N.; Lin, Y. W.; Song, J.; Cheng, Y.; et al. Engineering of Nebulized Metal–Phenolic Capsules for Controlled Pulmonary Deposition. *Adv. Sci.* **2020**, *7*, 1902650.

(13) Gause, K. T.; Yan, Y.; O'Brien-Simpson, N. M.; Cui, J.; Lenzo, J. C.; Reynolds, E. C.; Caruso, F. Codelivery of NOD2 and TLR9 Ligands via Nanoengineered Protein Antigen Particles for Improving and Tuning Immune Responses. *Adv. Funct. Mater.* **2016**, *26*, 7526–7536

(14) Cui, J.; De Rose, R.; Best, J. P.; Johnston, A. P. R.; Alcantara, S.; Liang, K.; Such, G. K.; Kent, S. J.; Caruso, F. Mechanically Tunable, Self-Adjuvanting Nanoengineered Polypeptide Particles. *Adv. Mater.* **2013**, *25*, 3468–3472

(15) Sexton, A.; Whitney, P. G.; Chong, S.-F.; Zelikin, A. N.; Johnston, A. P. R.; De Rose, R.; Brooks, A. G.; Caruso, F.; Kent, S. J. A Protective Vaccine Delivery System for In Vivo T Cell Stimulation Using Nanoengineered Polymer Hydrogel Capsules. *ACS Nano* **2009**, *3*, 3391–3400.

(16) Chong, S.-F.; Sexton, A.; De Rose, R.; Kent, S. J; Zelikin, A. N.; Caruso, F. A Paradigm for Peptide Vaccine Delivery Using Viral Epitopes Encapsulated in Degradable Polymer Hydrogel Capsules. *Biomaterials* **2009**, *30*, 5178–5186.

(17) Lian, X.; Fang, Y.; Joseph, E.; Wang, Q.; Li, J.; Banerjee, S.; Lollar, C.; Wang, X.; Zhou, H.-C. Enzyme–MOF (Metal–Organic Framework) Composites. *Chem. Soc. Rev.* **2017**, *46*, 3386–3401.

(18) Zhu, Q.; Pan, Q. Mussel-Inspired Direct Immobilization of Nanoparticles and Application for Oil–Water Separation. *ACS Nano* **2014**, *8*, 1402–1409.

(19) Deng, Y.; Qi, D.; Deng, C.; Zhang, X.; Zhao, D. Superparamagnetic High-Magnetization Microspheres with an $Fe_3O_4$@$SiO_2$ Core and Perpendicularly Aligned Mesoporous $SiO_2$ Shell for Removal of Microcystins. *J. Am. Chem. Soc.* **2008**, *130*, 28–29.

(20) Richardson, J. J.; Björnmalm, M.; Caruso, F. Technology-Driven Layer-by-Layer Assembly of Nanofilms. *Science* **2015**, *348*, aaa2491.

(21) Caruso, F.; Caruso, R. A.; Möhwald, H. Nanoengineering of Inorganic and Hybrid Hollow Spheres by Colloidal Templating. *Science* **1998**, *282*, 1111–1114.

(22) Rahim, M. A.; Kempe, K.; Mullner, M.; Ejima, H.; Ju, Y.; van Koeverden, M. P.; Suma, T.; Braunger, J. A.; Leeming, M. G.; Abrahams, B. F. et al. Surface-Confined Amorphous Films from Metal-Coordinated Simple Phenolic Ligands. *Chem. Mater.* **2015**, *27*, 5825–5832.

(23) Ulbrich, K.; Hola, K.; Subr, V.; Bakandritsos, A.; Tucek, J.; Zboril, R. Targeted Drug Delivery with Polymers and Magnetic Nanoparticles: Covalent and Noncovalent Approaches, Release Control, and Clinical Studies. *Chem. Rev.* **2016**, *116*, 5338–5431.

(24) Delplace, V.; Nicolas, J. Degradable Vinyl Polymers for Biomedical Applications. *Nat. Chem.* **2015**, *7*, 771–784.

(25) Jia, F.; Lu, X.; Wang, D.; Cao, X.; Tan, X.; Lu, H.; Zhang, K. Depth-Profiling the Nuclease Stability and the Gene Silencing Efficacy of Brush-Architectured Poly(ethylene glycol)–DNA Conjugates. *J. Am. Chem. Soc.* **2017**, *139*, 10605–10608.

(26) Ju, Y.; Cui, J.; Mullner, M.; Suma, T.; Hu, M.; Caruso, F. Engineering Low-Fouling and pH-Degradable Capsules through the Assembly of Metal-Phenolic Networks. *Biomacromolecules* **2015**, *16*, 807–814.

(27) Holten-Andersen, N.; Harrington, M. J.; Birkedal, H.; Lee, B. P.; Messersmith, P. B.; Lee, K. Y. C.; Waite, J. H. pH-Induced Metal-Ligand Cross-Links Inspired by Mussel Yield Self-Healing Polymer Networks with near-Covalent Elastic Moduli. *Proc. Natl. Acad. Sci. U. S. A.* **2011**, *108*, 2651–2655.

(28) Shin, E.; Lim, C.; Kang, U. J.; Kim, M.; Park, J.; Kim, D.; Choi, W.; Hong, J.; Baig, C.; Lee, D. W. Mussel-Inspired Copolyether Loop with Superior Antifouling Behavior. *Macromolecules* **2020**, *53*, 3551–3562.

(29) Yun, G.; Besford, Q. A.; Johnston, S. T.; Richardson, J. J.; Pan, S.; Biviano, M.; Caruso, F. Self-Assembly of Nano- to Macroscopic Metal–Phenolic Materials. *Chem. Mater.* **2018**, *30*, 5750–5758.

(30) Zhong, Q.-Z.; Li, S.; Chen, J.; Xie, K.; Pan, S.; Richardson, J. J.; Caruso, F. Oxidation-Mediated Kinetic Strategies for Engineering Metal–Phenolic Networks. *Angew. Chem., Int. Ed.* **2019**, *58*, 12563–12568.

(31) Chen, J.; Pan, S.; Zhou, J.; Zhong, Q.-Z.; Qu, Y.; Richardson, J. J.; Caruso, F. Programmable Permeability of Metal–Phenolic Network Microcapsules. *Chem. Mater.* **2020**, *32*, 6975–6982.

(32) Shi, Z.-H.; Li, N.-G.; Shi, Q.-P.; Tang, H.; Tang, Y.-P.; Li, W.; Yin, L.; Yang, J.-P.; Duan, J.-A. Synthesis and Structure–Activity Relationship Analysis of Caffeic Acid Amides as Selective Matrix Metalloproteinase Inhibitors. *Bioorg. Med. Chem. Lett.* **2013**, *23*, 1206–1211.

(33) Misra, K.; Maity, H. S.; Nag, A.; Sonawane, A. Radical Scavenging and Antibacterial Activity of Caffemides against Gram Positive, Gram Negative and Clinical Drug Resistance Bacteria. *Bioorg. Med. Chem. Lett.* **2016**, *26*, 5943–5946.

(34) Fu, J.; Cheng, K.; Zhang, Z.-m.; Fang, R.-q.; Zhu, H.-l. Synthesis, Structure and Structure–Activity Relationship Analysis of Caffeic Acid Amides as Potential Antimicrobials. *Eur. J. Med. Chem.* **2010**, *45*, 2638–2643.

(35) Uwai, K.; Osanai, Y.; Imaizumi, T.; Kanno, S.-i.; Takeshita, M.; Ishikawa, M. Inhibitory Effect of the Alkyl Side Chain of Caffeic Acid Analogues on Lipopolysaccharide-Induced Nitric Oxide Production in Raw264. 7 Macrophages. *Bioorg. Med. Chem.* **2008**, *16*, 7795–7803.

(36) Fancelli, D.; Abate, A.; Amici, R.; Bernardi, P.; Ballarini, M.; Cappa, A.; Carenzi, G.; Colombo, A.; Contursi, C.; Di Lisa, F. Cinnamic Anilides as New Mitochondrial Permeability Transition Pore Inhibitors Endowed with Ischemia-Reperfusion Injury Protective Effect in Vivo. *J. Med. Chem.* **2014**, *57*, 5333–5347.

(37) Chen, Z.; Digiacomo, M.; Tu, Y.; Gu, Q.; Wang, S.; Yang, X.; Chu, J.; Chen, Q.; Han, Y.; Chen, J. Discovery of Novel Rivastigmine-Hydroxycinnamic Acid Hybrids as Multi-Targeted Agents for Alzheimer's Disease. *Eur. J. Med. Chem.* **2017**, *125*, 784–792.

(38) Liu, Z.; Fu, J.; Shan, L.; Sun, Q.; Zhang, W. Synthesis, Preliminary Bioevaluation and Computational Analysis of Caffeic Acid Analogues. *Int. J. Mol. Sci.* **2014**, *15*, 8808–8820.

(39) Nomura, E.; Kashiwada, A.; Hosoda, A.; Nakamura, K.; Morishita, H.; Tsuno, T.; Taniguchi, H. Synthesis of Amide Compounds of Ferulic Acid, and Their Stimulatory Effects on Insulin Secretion in Vitro. *Bioorg. Med. Chem.* **2003**, *11*, 3807–3813.

(40) Hunneche, C. S.; Lund, M. N.; Skibsted, L. H.; Nielsen, J. Antioxidant Activity of a Combinatorial Library of Emulsifier– Antioxidant Bioconjugates. *J. Agric. Food Chem.* **2008**, *56*, 9258–9268.

(41) de Armas-Ricard, M.; Ruiz-Reyes, E.; Ramírez-Rodríguez, O. Caffeates and Caffeamides: Synthetic Methodologies and Their Antioxidant Properties. *Int. J. Med. Chem.* **2019**, *2019*, 2592609.

(42) Tarbell, D. S. Carboxylic Carbonic Anhydrides and Related Compounds. *Acc. Chem. Res.* **1969**, *2*, 296–300.

(43) Tarbell, D. S.; Leister, N. A. The Stability of Mixed Carboxylic-Carbonic Anhydrides. *J. Org. Chem.* **1958**, *23*, 1149–1152.

(44) Vaughan Jr, J. R.; Eichler, J. A. The Preparation of Optically-Active Peptides Using Mixed Carbonic—Carboxylic Acid Anhydrides. *J. Am. Chem. Soc.* **1953**, *75*, 5556-5560.

(45) Nakamura, K.; Nakajima, T.; Aoyama, T.; Okitsu, S.; Koyama, M. One-Pot Esterification and Amidation of Phenolic Acids. *Tetrahedron* **2014**, *70*, 8097–8107.

(46) DellaGreca, M.; Longobardo, L. Protection and Activation of Hydroxycinnamic Acids in Water. *ChemistrySelect* **2020**, *5*, 4588–4591.

(47) Li, L.; Li, Y.; Luo, X.; Deng, J.; Yang, W. Helical Poly(*N*-Propargylamide)s with Functional Catechol Groups: Synthesis and Adsorption of Metal Ions in Aqueous Solution. *React. Funct. Polym.* **2010**, *70*, 938–943.

(48) Chen, F. M. F.; Lee, Y.; Steinauer, R.; Benoiton, N. L. Mixed Anhydrides in Peptide Synthesis. A Study of Urethane Formation with a Contribution on Minimization of Racemization. *Can. J. Chem.* **1987**, *65*, 613–618.

(49) Pal, B.; Jaisankar, P.; Giri, V. S. Versatile Reagent for Reduction of Azides to Amines. *Synth. Commun.* **2004**, *34*, 1317–1323.

(50) Sever, M. J.; Wilker, J. J. Visible Absorption Spectra of Metal–Catecholate and Metal–Tironate Complexes. *Dalton Trans.* **2004**, 1061–1072.

(51) Rahim, M. A.; Björnmalm, M.; Bertleff-Zieschang, N.; Besford, Q.; Mettu, S.; Suma, T.; Faria, M.; Caruso, F. Rust-Mediated Continuous Assembly of Metal–Phenolic Networks. *Adv. Mater.* **2017**, *29*, 1606717.

(52) Sun, H.; Wong, E. H.; Yan, Y.; Cui, J.; Dai, Q.; Guo, J.; Qiao, G. G.; Caruso, F. The Role of Capsule Stiffness on Cellular Processing. *Chem. Sci.* **2015**, *6*, 3505–3514.

(53) Amoozgar, Z.; Yeo, Y. Recent Advances in Stealth Coating of Nanoparticle Drug Delivery Systems. *Wiley Interdiscip. Rev.: Nanomed. Nanobiotechnol.* **2012**, *4*, 219–233.

(54) Fan, W.; Yung, B.; Huang, P.; Chen, X. Nanotechnology for Multimodal Synergistic Cancer Therapy. *Chem. Rev.* **2017**, *117*, 13566–13638.

(55) Guo, J.; Suma, T.; Richardson, J. J.; Ejima, H. Modular Assembly of Biomaterials Using Polyphenols as Building Blocks. *ACS Biomater. Sci. Eng.* **2019**, *5*, 5578–5596.

(56) Lee, H. A.; Ma, Y.; Zhou, F.; Hong, S.; Lee, H. Material-Independent Surface Chemistry Beyond Polydopamine Coating. *Acc. Chem. Res.* **2019**, *52*, 704–713.

## Table of Contents Graphic